W, Z, PHOTON PHYSICS AND A SEARCH FOR NEW PARTICLES WITH THE UA2 DETECTOR

The UA2 Collaboration

Bern - Cambridge - CERN - Dortmund - Heidelberg - Melbourne - Milano - Orsay (LAL) - Pavia - Perugia - Pisa - Saclay (CEN)

presented by

Monica Pepe
CERN, Geneva, Switzerland

ABSTRACT

During the 1988–1989–1990 runs the UA2 experiment has collected a data sample corresponding to an integrated luminosity of 13 pb^{-1}. The decays $W^{\pm} \rightarrow e^{\pm}\nu$ and $Z \rightarrow e^{+}e^{-}$ have been studied : results are given on the measurement of the production cross sections times branching ratio and of the W and Z masses. The measurement of the inclusive cross section for direct photon production is presented. Recent results on the search for new particles and rare W decays are discussed : searches are made for the rare decay $W^{\pm} \rightarrow \pi^{\pm}\gamma$, for scalar leptoquark pair production and for top quark decay into charged Higgs particles $H^{\pm}$.

1 Introduction

The data sample collected by the UA2 experiment between 1988 and 1990 at the CERN $\overline{p}p$ Collider ($\sqrt{s} = 630\ GeV$) corresponds to an integrated luminosity of $13.0 \pm 0.7\ pb^{-1}$. The upgraded UA2 detector is optimized for the identification of electrons and the indirect detection of neutrinos through the measurement of missing transverse momentum.

This report is organized as follows : Section 2 gives a brief description of the UA2 detector. The final results on the study of the production properties and on the measurement of the masses of W and Z bosons are presented in Section 3. The direct photon production cross section measurement is described in Section 4, while Section 5 presents the results from the search for new particles and rare W decays.

The analyses presented are based on the full sample of data collected between 1988 and 1990, except for the single photon analysis which is based on the data collected during the 1988-1989 running period only, corresponding to an integrated luminosity of $7.4 \pm 0.4\ pb^{-1}$.

2 The UA2 Apparatus

The UA2 detector (Fig. 1) [1] provides full azimuthal coverage around the interaction region in the pseudorapidity range $-3 < \eta < 3$ and consists of a central tracking detector surrounded by electromagnetic and hadronic calorimeters [2].

The calorimeter is divided into a central part (CC) with $|\eta| < 1$ and two end cap regions (EC) reaching $|\eta| = 3$. All calorimeters use the sampling technique, with a tower structure and wavelength shifter readout. The granularity is $\Delta\theta \cdot \Delta\phi = 10° \cdot 15°$ in the CC and $\Delta\eta \cdot \Delta\phi = 0.2 \cdot 15°$ in the EC, except for the two cells closest to the beam axis where $\Delta\eta = 0.3$ and 0.5 respectively. The electromagnetic compartments are multi-layer lead-scintillator sandwiches with a total thickness of 17 radiation lengths (r.l.) in the CC and varying between 17.1 and 24.4 r.l. in the EC, depending on the polar angle θ. The hadronic compartments are multi-layer iron-scintillator sandwiches, 4 absorption lengths (a.l.) deep in the CC and 6.5 a.l. deep in the EC.

Clusters are reconstructed in the calorimeter by joining all cells with an energy greater than 400 MeV sharing a common edge. Clusters with a small lateral size and a small energy leakage into the hadronic compartments are marked as electromagnetic clusters.

The central detector, used to determine the position of the event vertex and to reconstruct charged particle tracks, consists of two silicon pad counter arrays around the beam at radii of 2.9 cm and 14.8 cm. A cylindrical drift chamber is located between the two silicon detectors. Beyond the outer silicon layer there is a transition radiation detector, consisting of two sets of radiators and proportional chambers, followed by a scintillating fibre detector which provides track

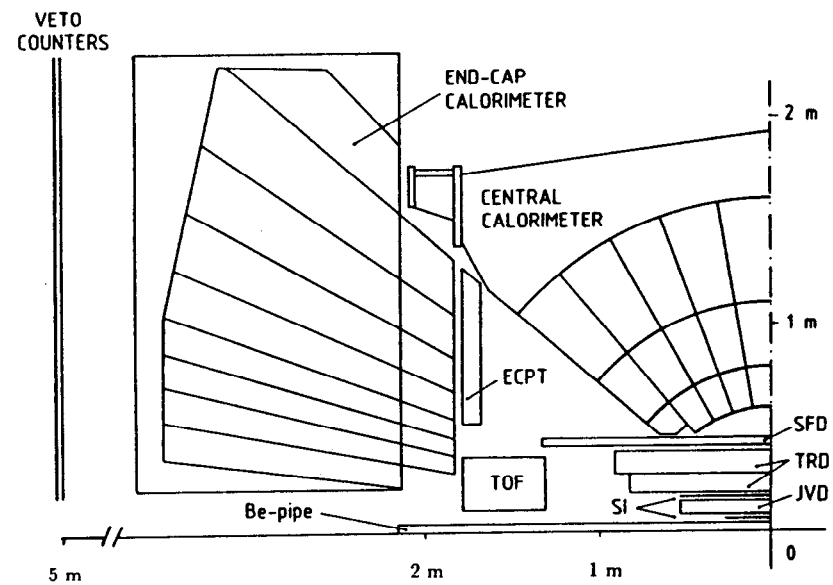

Figure 1: *Longitudinal view of one quadrant of the UA2 detector.*

segments in the first six stereo triplets of fibres and localizes the beginning of electromagnetic showers in front of the CC in the last two stereo triplets, located after a 1.5 r.l. thick lead converter.

In the forward regions, $|\eta| > 1$, tracking and preshower measurements are provided by three stereo triplets of proportional tubes placed in front of the end cap calorimeters. The first two triplets are used as a tracking device, while the last triplet, placed after a 2 r.l. thick iron and lead converter, acts as a preshower detector. Two sets of time-of-flight hodoscopes are located at small angles with respect to the beam. Their function is to define a minimum bias trigger and to provide an independent vertex measurement. Finally, two planes of large area scintillation counters cover the back sides of the end cap calorimeters. Events caused by beam halo particles are rejected in the analysis by detecting charged particles giving an early signal in these counters with respect to the beam crossing time.

For electron analyses, the detector can logically be divided into three acceptance regions in which efficiency, rejection and resolution are studied separately : central (non-edge) ($|\eta| < 0.8$), central (edge) ($0.8 < |\eta| < 1.0$) and forward ($1.0 < |\eta| < 1.6$).

The event selection is based on trigger requirements implemented in a three-level trigger system [3] based mainly on information from the calorimeters. The first level uses analog sums of the signals from the photomultipliers of the calorimeter cell compartments. At the second level, electromagnetic and hadronic clusters are reconstructed in a special-purpose processor using information from a fast digitization of the calorimeter cell signals. A complete calorimeter reconstruction is performed in the third level processors using the final digitization and the full set of calibration constants.

3 W and Z Properties

The W and Z bosons are identified by their leptonic decays $W^{\pm} \to e^{\pm}\nu$ and $Z \to e^+e^-$. The measurement of the products of cross section times branching ratio [4], $\sigma_W^e = \sigma(\bar{p}p \to W+X)\cdot B(W^{\pm} \to e^{\pm}\nu)$ and $\sigma_Z^e = \sigma(\bar{p}p \to Z+X)\cdot B(Z \to e^+e^-)$, can be compared to recent theoretical predictions which include complete $O(\alpha_s^2)$ calculations [5]. The ratio σ_W^e/σ_Z^e gives an indirect measurement of the total width of the W boson, Γ_W. The measurement of Γ_W can be used to establish a lower limit on the top quark mass which is independent of the top decay mode. The W and Z boson masses are measured [6]. The ratio m_W/m_Z can be used to evaluate $sin^2\theta_W$ and, in combination with the precise m_Z measurement from LEP, to obtain a precise value of m_W.

3.1 Electron and neutrino identification

The selection of electromagnetic clusters is obtained from calorimeter information alone. Electron candidates are defined by the following standard requirement :

- A track must be associated with the electromagnetic cluster. The track must originate from a reconstructed vertex which is not displaced from the centre of the detector by more than 250 mm along the beam direction.
- A preshower cluster must be reconstructed which is consistent with the position of the electron candidate track.
- The lateral and longitudinal profile of the shower in the calorimeter is required to be consistent with that expected from an electron incident along the track trajectory as measured in test beams.

Energy corrections are applied according to the precise electron direction and impact point in the calorimeter based on data obtained from 40 GeV test beam electrons. The corrected energy is used together with the direction given by the tracking detectors to define the electron momentum, $\vec{p}^e$. The overall scale of the energy calibration for electrons is controlled to the level of 1% for the central (non-edge) cells.

The presence of neutrinos in $W \to e\nu$ decays is deduced by measuring the electron energy and the energies of all other particles (generally hadrons) in the event. The missing transverse momentum ($\vec{\not{p}}_T$) is attributed to the undetected neutrino:

$$\vec{p}_T^{\,\nu} \equiv \vec{\not{p}}_T = -\vec{p}_T^{\,e} - \vec{p}_T^{\,had}$$

Here $\vec{p}_T^{\,e}$ is the reconstructed transverse momentum of the electron candidate and $\vec{p}_T^{\,had}$ is the total transverse momentum of the recoil particles, calculated as

$$\vec{p}_T^{\,had} = \left(\sum E_{cell}\hat{v}_{cell}\right)_T$$

where $\hat{v}_{cell}$ is a unit vector from the interaction vertex to the centre of a calorimeter cell, E_{cell} is the energy in that cell, and the sum extends over all cells in the calorimeter ($-3 < \eta < 3$) excluding the cells assigned to the electron.

3.2 Event selection

The requirements for a W candidate are that $p_T^e > 20\ GeV$, $p_T^{\nu} > 20\ GeV$ and $m_T > 40\ GeV$, where $m_T \equiv \sqrt{2p_T^e p_T^{\nu}(1 - cos\phi^{e\nu})}$ and $\phi^{e\nu}$ is the azimuthal separation between the measured electron and neutrino directions. The p_T^e and p_T^{ν} spectra of the final sample (3559 events) are shown in Fig. 2. The background contamination is estimated as described in ref. [4] : the QCD background is determined to be $0.5 \pm 0.2\%$ of the W candidates, while the background from

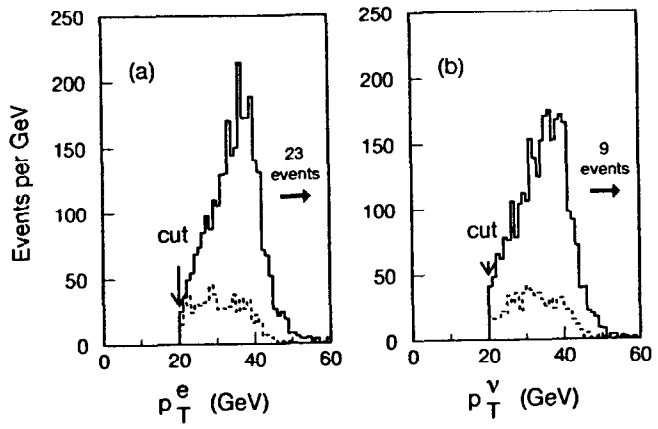

Figure 2: *The p_T^e (a) and p_T^ν (b) spectra for W candidates in the central (solid) and forward (dashed) acceptance regions.*

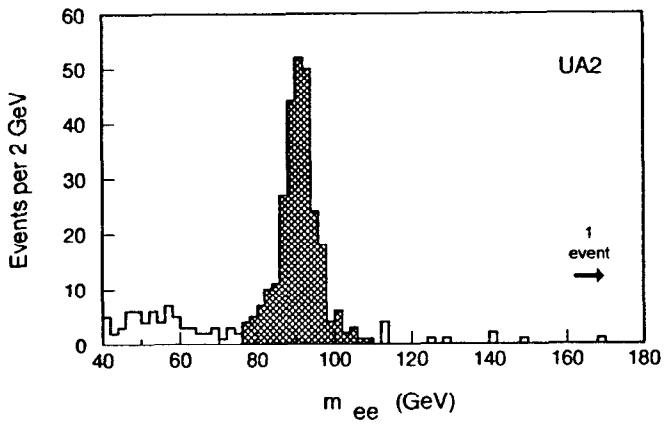

Figure 3: *The invariant mass spectrum of electron pairs passing final identification cuts. The range of m_{ee} used to select the final Z candidates is indicated by the shaded region.*

the process $W \to \tau\nu$, $\tau \to e\nu\bar{\nu}$ is estimated to be $3.8 \pm 0.1\%$ ($3.3 \pm 0.3\%$) in the central (forward) region.

The Z candidates are selected by requiring an electron with $p_T^e > 20\ GeV$ and an additional electron with $p_T^e > 15\ GeV$. The second electron may pass the looser track or preshower requirements described in ref. [4]. Figure 3 shows the invariant mass spectrum of the selected electron pairs (m_{ee}). The final sample of 269 events is obtained by requiring $76 < m_{ee} < 110\ GeV$. The QCD (two jet events) and Drell-Yan background in the signal region is estimated to be 3.4 ± 0.3 events.

3.3 Cross section measurement

The W cross section is determined in each acceptance region from the equation :

$$\sigma_W^e = \frac{N_W - N_{QCD} - N_\tau}{\epsilon\ \eta\ L}$$

where N_W is the number of observed W candidates, N_{QCD} is the estimated QCD background, N_τ is the estimated contribution from $W \to \tau\nu$, η is the geometrical acceptance, ϵ is the total efficiency and L is the integrated luminosity corresponding to the data sample.

The cross sections for Z production is calculated as

$$\sigma_Z^e = \frac{(N_Z - N_{QCD})(1 - f_{\gamma^*})}{\epsilon\ \eta\ L}$$

where N_Z is the observed number of Z candidates, N_{QCD} is the QCD background estimate, η is the acceptance and L is the integrated luminosity. The correction constant $f_{\gamma^*} = 1.65\%$ compensates for the contribution from single photon exchange and $\gamma^* Z$ interference, so that the final result can be compared to predictions based on the Z propagator alone.

The final cross sections are obtained by combining the results from the individual subsamples in the different acceptance regions with weights according to the product of acceptance and efficiency :

$$\sigma_W^e = 682 \pm 12(stat) \pm 40(syst)\ pb$$
$$\sigma_Z^e = 65.6 \pm 4.0(stat) \pm 3.8(syst)\ pb\,.$$

The measurements are compared in Fig. 4 with the theoretical predictions at the Born level and including $O(\alpha_s)$ and $O(\alpha_s^2)$ corrections as a function of the top quark mass : the QCD corrected predictions are in good agreement with the UA2 measurements. The top mass limits from LEP (model independent) and CDF (model dependent) are indicated on the abscissae. There is some sensitivity to the choice of structure functions : the curves have been obtained with the parton

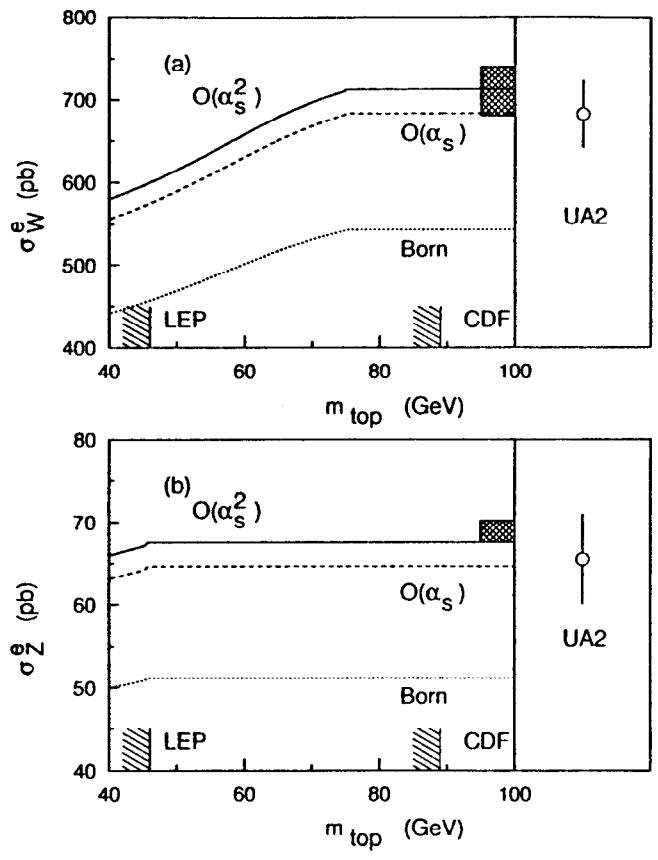

Figure 4: *Comparison of σ_W^e (a) and σ_Z^e (b) with the theoretical predictions as a function of the top quark mass.*

density parameterizations of HMRSB [7] and the shaded bands at the right sides of the figures show the range of variation over several structure function sets [8]. The structure function uncertainties on σ_W^e are comparable to the experimental errors and to the second order QCD corrections. The dependence on the top quark mass of σ_W^e and σ_Z^e comes from the top contribution to the total widths.

3.4 Measurement of Γ_W

An indirect measurement of Γ_W can be extracted from the cross section ratio σ_W^e/σ_Z^e. When one computes the ratio $R = \sigma_W^e/\sigma_Z^e$, the systematic errors are smaller than those on the individual cross sections. The luminosity error cancels completely, and there are also large cancellations of the error on the efficiency. The result is

$$R = \sigma_W^e/\sigma_Z^e = 10.4 \pm^{0.7}_{0.6} (\text{stat}) \pm 0.3(\text{syst})$$

where the correlations of all of the factors have been taken into account with a Monte Carlo error propagator to obtain the final errors. Theoretically, this ratio can be expressed as

$$R = \frac{\sigma_W}{\sigma_Z} \frac{\Gamma(W^\pm \to e^\pm \nu)}{\Gamma(Z \to e^+e^-)} \frac{\Gamma_Z}{\Gamma_W}$$

where the first two ratios on the right can be reliably computed within the Standard Model. The values of σ_W and σ_Z come from the $O(\alpha_s^2)$ calculation [5], where the mass values $m_W = 80.14 \pm 0.27\ GeV$ [6, 9] and $m_Z = 91.175 \pm 0.021\ GeV$ [10] are used, along with the corresponding value of $sin^2\theta_W = 0.2274$ [6]. Although many uncertainties cancel in the ratio, there is still some dependence on the boson masses and structure functions. The dominant theoretical error on R results from the structure function dependence of σ_W/σ_Z which arises from the uncertainty in the ratio d/u of parton density functions for down and up valence quarks, since W and Z bosons couple differently to the two types of quarks. An overall error of $\pm 3\%$ is assigned to the theoretical uncertainties in the calculation of σ_W/σ_Z. In combination with the value of $\Gamma_Z = 2.487 \pm 0.010\ GeV$ from LEP [10], one obtains

$$\Gamma_W = 2.10 \pm^{0.14}_{0.13} (stat) \pm 0.06(syst) \pm 0.06(SF)\ GeV\ = 2.10 \pm 0.16\ GeV.$$

Similar measurements have been reported by CDF [11] and UA1 [12]. The total width Γ_W is sensitive to any decay modes of the W whether they are detected or not. In particular, the presence of a top quark lighter than the W would result in a larger width, so Γ_W can be used to set a lower limit on m_{top}. The best direct search for the top quark restricts its mass to $m_{top} > 89\ GeV$ [13]. This limit, however, requires that the top has the expected semileptonic branching ratio and could be invalid, for example, if the top decays via a charged Higgs

boson. Apart from Γ_W measurements, the best limits on m_{top} which do not depend on the decay modes of the top come from LEP, and establish a limit well below m_W: $m_{top} > 46\ GeV$ [10]. Figure 5 shows the prediction for Γ_W as a function of m_{top} including mass dependent QCD corrections. From the UA2 measurement of the width alone, one obtains a limit of $m_{top} > 53\ GeV$ at the 95% CL. The combination of UA2, CDF, and UA1 gives $\Gamma_W = 2.15 \pm 0.11\ GeV$ which corresponds to $m_{top} > 55\ GeV$ at the 95% CL.

3.5 Determination of m_W and m_Z

The method used to determine m_W and m_Z is described in ref. [6] : the W mass is measured from fits to transverse mass and momentum spectra in $W^{\pm} \rightarrow e^{\pm}\nu$ decays, while the Z mass is determined from the two electron invariant mass distribution in $Z \rightarrow e^+e^-$ decays. The calibration scale errors largely cancel in the ratio of the two masses, so a precise value of m_W is obtained by rescaling the ratio with the m_Z value from LEP.

This analysis uses only W events in which the electron is in the central calorimeter. Additional fiducial cuts are applied so that the edge cells and the cell borders are excluded in order to obtain highest quality energy reconstruction. The electron must pass the standard criteria described in section 3.2. In addition, the transverse mass m_T is required to be between 40 and 120 GeV and the requirement $p_T^W < 20\ GeV$ is imposed because the p_T^ν resolution is degraded in events with large amounts of hadronic energy. This leaves 2065 events. Since the longitudinal momentum of the neutrino is not measured, the W mass must be obtained by fitting to a transverse kinematical variable such as p_T^e, p_T^ν or m_T. The fitting is restricted to the range $60-120\ GeV$ for the m_T fits and $30-60\ GeV$ for the p_T^e and p_T^ν fits. The three distributions are not independent, so they cannot be combined to give a more precise result. The result of the m_T fit,

$$m_W = 80.84 \pm 0.22(stat) \pm 0.17(syst) \pm 0.81(scale)\ GeV$$

is taken because it has the smallest errors, while the fits to p_T^e and p_T^ν provide a useful cross check of the measurement systematics. The result for the m_T fit is shown in Fig. 6.

In selecting the samples for the Z mass determination, it is important that the energy scale in the mass measurement comes from the same fiducial volume as defined for the W events. In this way there is maximal cancellation of the dominant calibration errors in computing the ratio m_W/m_Z. In a first Z sample both electron candidates (selected as in section 3.2) are required to be in the fiducial volume of the central calorimeter. The mass of the electron candidate pair m_{ee} is calculated from the corrected momenta of the electrons, and it is required to be between 70 and 120 GeV. This yields a sample of 95 events. A second independent Z sample is obtained as described in ref. [6] : one electron is required to be in the central fiducial volume while the other one must be

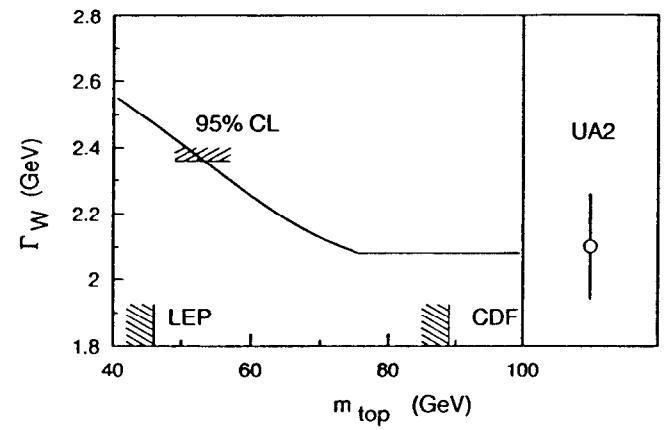

Figure 5: *The final result for Γ_W is compared with the Standard Model predictions for Γ_W as a function of m_{top}.*

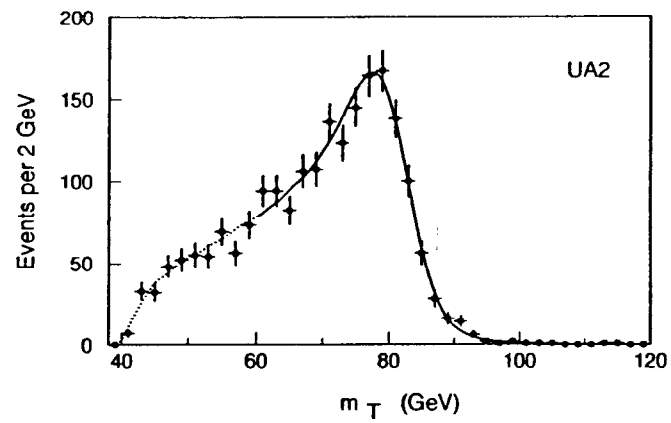

Figure 6: *Fit for m_W to the m_T spectrum. The points show the data, while the curves show the fit result with the solid line indicating the range over which the fit is performed.*

outside, either in the forward or edge region or in the cell borders of the central calorimeter. The mass is then calculated by rescaling the momentum of the non-fiducial electron until the total event momentum balances along the ξ axis, where ξ is the outer bisector of the angle between the two electrons in the transverse plane. By this procedure, the energy scale of the central calorimeter is transferred to the second electron. This "p_T-constrained" mass is required to be between 70 and 120 GeV, yielding a sample of 156 events. This sample has poorer mass resolution than the central Z sample, but with the larger number of events it makes a significant contribution to the Z mass measurement. The fits to m_Z are shown in Fig. 7. The results from the two samples are in good agreement and the combined result is

$$m_Z = 91.74 \pm 0.28(stat) \pm 0.12(syst) \pm 0.92(scale)\ GeV$$

after correcting for the effect of radiative decays and of the underlying event.

The systematic uncertainties on the m_W and m_Z measurements are summarized in Table 1. A discussion of the individual contributions can be found in ref. [6].

	$\delta m_W(m_T)$	$\delta m_W(p_T^e)$	$\delta m_W(p_T^\nu)$	$\delta m_Z(CC)$	$\delta m_Z(p_T con)$
struct. fun.	85	135	105	-	-
e en. resol.	75	100	75	35	35
ν scale	70	-	140	-	-
p_T^W and p_T^{had}	60	120	90	-	-
underl. event	30	50	-	50	50
fit procedure	30	40	40	-	-
rad. decays	30	50	20	50	50
e eff. vs p_T^e	30	40	30	-	-
$u_{\parallel}$ effect	25	95	350	-	-
p_T constr.	-	-	-	-	100
total syst.	160	240	420	80	130

Table 1: *The size (in MeV) of the systematic uncertainties in measuring m_W and m_Z.*

The scale errors from the calorimeter calibration cancel in the ratio m_W/m_Z aside from a residual $\pm 80\ MeV$ effect of possible nonlinearities in the calorimeter energy response. In addition, some of the systematic errors contain some correlations which are taken into account. The ratio

$$m_W/m_Z = 0.8813 \pm 0.0036(stat) \pm 0.0019(syst)$$

can be multiplied by the LEP value for m_Z [10] to give a more precise value for the W mass :

$$m_W = 80.35 \pm 0.33(stat) \pm 0.17(syst)\ GeV$$

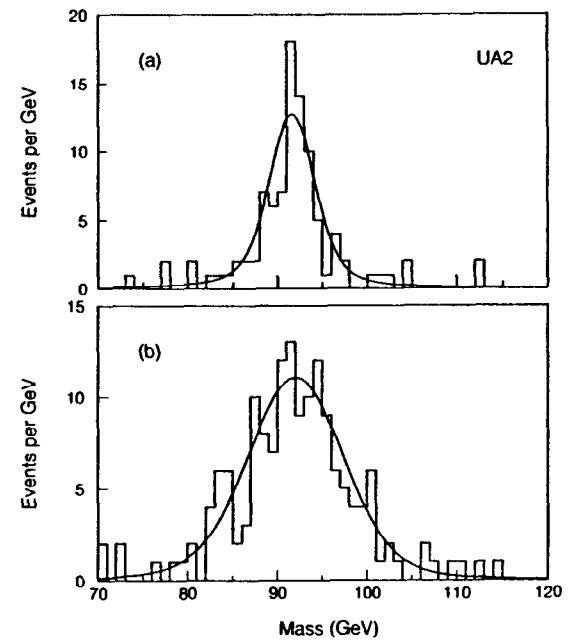

Figure 7: *Fits for m_Z to (a) the central sample and (b) the p_T-constrained sample. The curves show the fits, while the histograms show the data.*

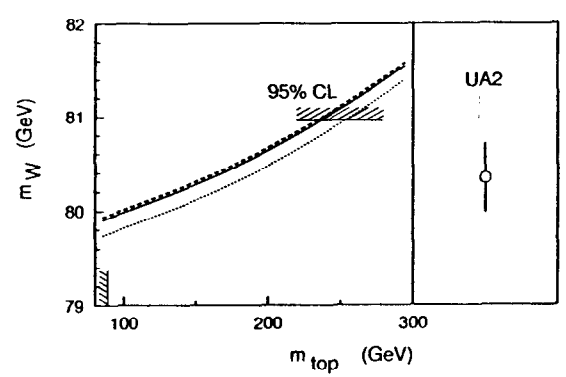

Figure 8: *The final result for m_W is compared with the Standard Model predictions for m_W as a function of m_{top} and m_H. The dashed, solid and dotted curves correspond to Higgs masses of 50 GeV, 100 GeV, and 1000 GeV, respectively.*

Using the Sirlin [14] convention $sin^2\theta_W \equiv 1 - m_W{}^2/m_Z{}^2$ the value

$$sin^2\theta_W = 0.2234 \pm 0.0064 \pm 0.0033$$

is obtained. This value is in agreement with the result derived from low energy data [15]. Combining the results of UA2 and CDF a value $sin^2\theta_W = 0.2274 \pm 0.0052$ is obtained.

Within the Standard Model, the ratio m_W/m_Z is determined at the Born level from the parameters α, G_μ, and m_Z. Radiative corrections can modify this prediction significantly. In the minimal Standard Model, these corrections depend strongly (quadratically) on the mass of the top quark (m_{top}) and weakly (logarithmically) on the mass of the Higgs boson (m_H). Consequently, the measurement of m_W/m_Z can be used to place some (model dependent) bounds on m_{top}, as shown in Fig. 8. The results are $m_{top} = 160 \pm^{50}_{60}\ GeV$ ($m_{top} = 130 \pm^{40}_{50}\ GeV$) for $m_H = 100\ GeV$, and $m_{top} < 250 GeV$ ($m_{top} < 215 GeV$) at the 95% CL for $m_H < 1\ TeV$ from the UA2 result alone (or combining the results of UA2 and CDF).

4 Direct Photon Production

The direct production of isolated large transverse momentum photons in hadron-hadron collisions is a convenient way to study the constituents of hadronic matter and their interactions. A measurement of the direct photon cross section [16] provides a test of QCD with the advantage that the photon transverse momentum is not affected by fragmentation effects, resulting in experimental uncertainties which are considerably smaller than those obtained, for instance, in the measurement of a jet cross section. Next-to-leading order calculations are also available [17] and can be directly compared to the experimental results.

The main source of background is the production of high transverse momentum hadron jets since they often contain one or more π^0 (or η) mesons which decay into photon pairs that are not resolved by the calorimeter. This background has a cross section approximately four orders of magnitude higher than the direct photon signal. The latter, however, results in isolated electromagnetic clusters, whereas the background from hadron jets is accompanied by jet fragments, so that an "isolation requirement" is very effective in reducing the background in the signal sample.

4.1 Event selection and background subtraction

The present analysis is based on events selected using the W trigger and having an electromagnetic cluster well contained in a fiducial region of the central calorimeter ($|\eta| < 0.76$). Only events with a single reconstructed $\bar{p}p$ interaction vertex are considered. In addition the events must contain at least one cluster having the characteristics expected for an isolated single photon :

a. The lateral and longitudinal profiles of the cluster are required to be consistent with that expected for a single isolated electron or photon.

b. The absence of any charged track in front of the calorimeters, as ensured by pulse height requirements imposed on any silicon pad or pad cluster present in either silicon counter within a window of $\Delta\eta < 0.2$ and $\Delta\phi < 15°$ about the cluster axis (defined by the line joining the interaction vertex to the cluster centroid).

c. At most one preshower signal in a cone $\sqrt{\Delta\phi^2 + \Delta\eta^2} < 0.265$ about the cluster axis.

A total of 26086 photon candidates with $p_T > 15\ GeV$ are found with a global efficiency of $\varepsilon_c = 0.443 \pm 0.009$. This value does not include effects associated with photon conversions in the preshower detector. The applied isolation criteria reject a large fraction of π^0's and η's while retaining direct photons. The residual background contamination is measured and subtracted on a statistical basis, by considering the fraction α of photons in the sample that initiate showers in the converter of the preshower detector. A converted photon candidate is defined by the observation of a signal in the preshower detector, otherwise the photon candidate is referred to as unconverted. In order to compute α, all the efficiencies which have a different value for converted and unconverted photon candidates have been taken into account, as discussed in ref. [16], to determine the true numbers of converted (N_c^{true}) and of unconverted (N_u^{true}) photons from the numbers of observed photon candidates. The conversion probability α in the sample is then computed as :

$$\alpha = \frac{N_c^{true}}{N_c^{true} + N_u^{true}} \ .$$

The conversion probability ε_γ of an incident single photon is evaluated as a function of the photon energy using the EGS shower simulation programme [18]. The simulation has been tuned to describe correctly the response to test beam electrons of 10 and 40 GeV and to electrons from W decays. The total systematic error on ε_γ is estimated to decrease with energy from 2.4% to 2.0%. The multiphoton conversion probability ε_π for photon pairs produced by π^0 and η decays is calculated using ε_γ for each photon and assuming that the ratio between the number of η and π^0 is 0.6 and p_T independent [19]. The systematic error for ε_π is mainly due to the uncertainty in the two-photon angular resolving power and ranges from 2.7% to 1.5% with increasing π^0 energy. The component of multi-π^0 states in the background has turns out to be highly suppressed by the preshower isolation requirement [16]. The calculated values of ε_π and ε_γ are compared in Fig. 9 with the measured conversion probability α as a function of the photon energy E_γ.

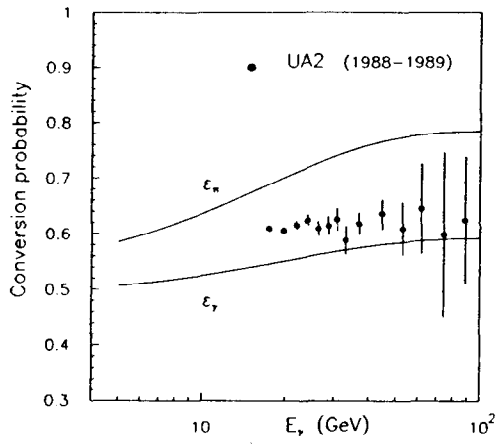

Figure 9: *Conversion fraction for photon candidates. The curves labeled ε_γ and ε_π are the conversion probabilities for single photons and multiphoton background, respectively.*

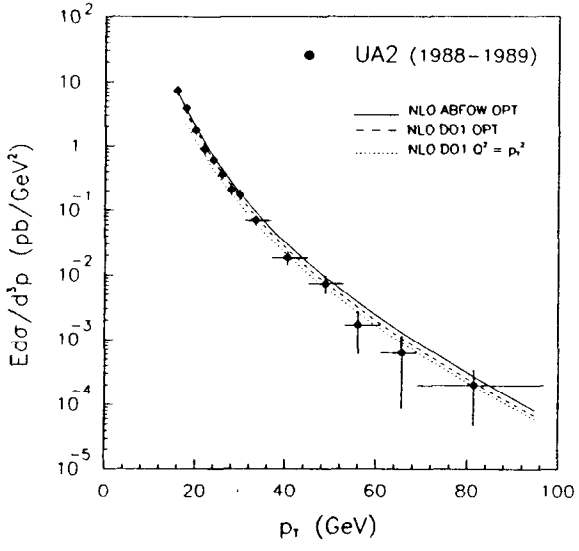

Figure 10: *The invariant differential cross section for direct photon production is compared with the QCD calculation of ref. [16] with two different sets of structure functions [19], namely Duke–Owens set 1 (DO1) and Aurenche et al. (ABFOW) with an optimized Q^2 scale (OPT) and $Q^2 = p_T^2$.*

The fraction of multiphoton events in the sample is computed from the values of α, ε_γ, ε_π :

$$b(p_T) = \frac{\alpha - \varepsilon_\gamma}{\varepsilon_\pi - \varepsilon_\gamma}$$

The remaining background caused by beam halo particles has been estimated to be less than 1% of the photon candidate sample and has been neglected. $W \to e\nu$ decays are expected to contribute at most 30 events in the p_T interval between 20 and 45 GeV as a result of inefficiencies in the electron track reconstruction. This contribution corresponds to 0.2% of the photon candidate events in the same p_T range.

4.2 Inclusive cross section

The invariant inclusive cross section for direct photon production is evaluated from

$$E\frac{d\sigma}{d^3p} = \frac{N_\gamma(p_T)\cdot[1 - b(p_T)]}{2\pi\, p_T\, \Delta p_T\, L\, \varepsilon_c\, A(p_T)}$$

where $N_\gamma(p_T)$ is the number of photon candidates in a p_T-bin of width Δp_T, $b(p_T)$ is the background fraction in that bin, $L = 7.4 \pm 0.4\ pb^{-1}$ is the integrated luminosity corresponding to the data sample, ε_c is the efficiency of the selection criteria for detecting direct photon events and $A(p_T)$ is the geometrical acceptance.

The results are compared to next-to-leading order QCD calculations [17] performed using different sets of structure functions [20]. In addition, the isolation cut used in the selection of the data suppresses the bremsstrahlung contribution from final state quarks, so that this effect is not included in the QCD calculation. The p_T distribution of the data together with the QCD expectations is shown in Fig. 10. The error bars indicate the statistical and p_T dependent systematic uncertainties added in quadrature. The latter arise from the uncertainties in the preshower isolation efficiency and in the Monte Carlo evaluation of ε_γ and ε_π, and from the difference in the energy reconstruction for converted and unconverted photons [16]. The overall p_T independent systematic error is 9%. Within uncertainties the data agree well with the QCD predictions but do not distinguish among the different structure function sets.

A comparison between the inclusive cross sections for direct photons and jets at $\eta = 0$ [21] is shown in Fig. 11. The errors shown include statistical and p_T dependent systematic errors added in quadrature. The overall p_T independent systematic error for the inclusive jet cross section is 32%.

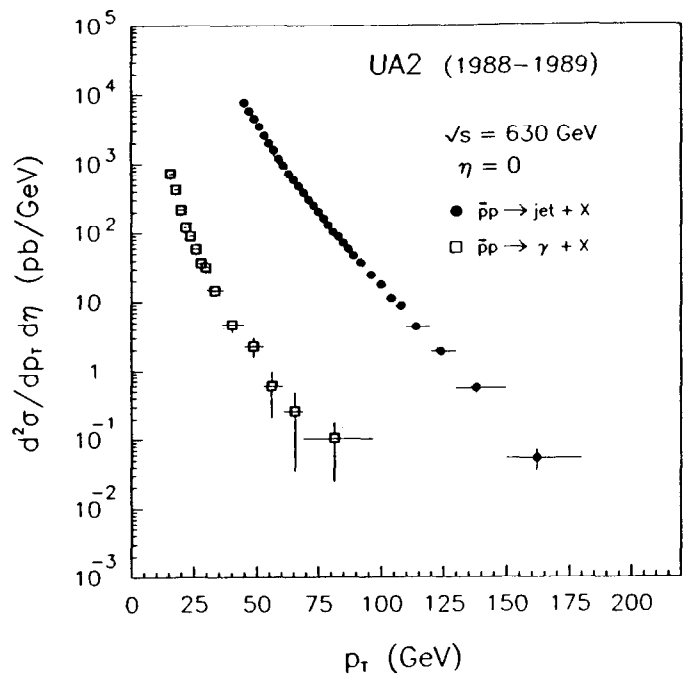

Figure 11: *The differential cross sections for direct photon production and jet production [20] are compared at $\eta = 0$.*

5 Search for New Particles

A search has been made for new particles and rare W decays. No evidence is found for the process $W^{\pm} \to \pi^{\pm}\gamma$ and upper limits on the ratio of the partial widths $R = \Gamma(W^{\pm} \to \pi^{\pm}\gamma) \,/\, \Gamma(W^{\pm} \to e^{\pm}\nu)$ and on the branching ratio $Br(W^{\pm} \to \pi^{\pm}\gamma)$ are derived [22].

A search has been made for scalar leptoquark pair production [23] followed by the decay of the leptoquark into a quark and either an electron or a neutrino. A lower limit has been determined for the mass of a first generation scalar leptoquark.

In the search for charged Higgs ($H^{\pm}$) from top quark decay in UA2 [24], the observed number of hadronic τ decays is compared to the number expected from $W^{\pm} \to \tau^{\pm}\nu$ decay under the assumption of $e-\tau$ universality. No excess of events is observed, excluding the process $t \to H^{+}b$, $H^{+} \to \tau\nu$ and its charge conjugate in a region of the (m_H, m_{top}) plane.

5.1 Limit on the decay $W^{\pm} \to \pi^{\pm}\gamma$

For the charged IVB, the UA2 experiment has observed the decay $W^{\pm} \to e^{\pm}\nu$ and the hadronic decay in the quark–antiquark channel [25]. In the same experiment a search has also been made for the decay $W^{\pm} \to \pi^{\pm}\gamma$. In the framework of the Standard Model this decay is highly suppressed and its rate is estimated to be [26] less than $3 \cdot 10^{-8}$ of the $W^{\pm} \to e^{\pm}\nu$ decay rate.

However, if one extends to W decays the method used to calculate the $\pi^{\circ} \to \gamma\gamma$ amplitude [27, 28], much larger values of R are obtained, corresponding to a branching ratio of the order of 0.1 for the decay $W^{\pm} \to \pi^{\pm}\gamma$. Such a large value has been questioned by several theoretical papers [29]. Furthermore, the UA1 Collaboration has obtained the limit [30] $R < 5.8 \cdot 10^{-2}$ (95% CL). The present result improves the experimental limit by more than an order of magnitude.

The online selection of the data was based on the trigger requirements for photon candidates [16]. The signature of the decay $W^{\pm} \to \pi^{\pm}\gamma$ is given by a photon and a charged pion opposite in azimuth with an invariant mass compatible with the W mass. A sample of events containing a photon candidate has been selected as in section 4.1. The photon candidates are required to have $p_T^{\gamma} > 20\ GeV$. The associated pion is identified by requiring the presence of an azimuthally opposite cluster in the region $\Delta\phi > 150°$ with respect to the photon direction. Only pion candidates with $p_T^{\pi} > 20\ GeV$ and $|\eta_{\pi}| < 2.0$ are retained. The selected sample contains 4435 events.

A Monte Carlo event sample has been generated using a special version of the PYTHIA 5.4 event generator [31] modified to include the decay $W^{\pm} \to \pi^{\pm}\gamma$ [32]. The generated events have been processed through full calorimeter and silicon detector simulations. The detector response to the single pion in the final state was simulated using a parametrization obtained from single charged pions as measured in test beams. The Monte Carlo events have been analyzed

using the same selection criteria given above and have been used for a qualitative comparison with the observed distributions and to compute the acceptance and the efficiencies of the selection criteria.

The background in the $W^{\pm} \rightarrow \pi^{\pm}\gamma$ search is mainly due to two QCD processes : the first is direct photon production, where an associated jet is misidentified as a single charged pion, and the second is the production of two jet events in which one jet fakes the photon and the other is taken as a single pion. Calorimeter and silicon detector information, which are well understood from test beam studies, are used to distinguish QCD jets from single pions as follows :

- A 40 GeV single pion is expected to induce a shower which is contained in a three-by-three group of calorimeter cells around the impact point. The requirement $N_{cells} \leq 9$ is therefore applied, where N_{cells} is the number of cells belonging to the pion candidate cluster.

- The *profile* ρ of a calorimeter cluster is defined as $\rho = (E_1 + E_2)/E_{tot}$, where the numerator corresponds to the sum of the energies of the two highest energy cells in the cluster and the denominator is the total energy of the cluster. Since single pions are expected to have high values of ρ, the requirement $\rho \geq 0.75$ is applied.

- A charged pion is expected to appear as a "mono-track" jet. The presence of a single charged track pointing to the pion candidate cluster is ensured by pulse height requirements imposed on the silicon counters, within a window of $\Delta\eta < 0.2$ and $\Delta\phi < 15°$ around the cluster axis.

- The invariant mass $M_{\gamma\pi}$ of the $\gamma\pi$ system must be consistent with the W mass. The $M_{\gamma\pi}$ distributions in the data and Monte Carlo samples are shown in Fig. 12 (a) and (b) respectively for the events passing all the previous criteria. A Gaussian fit to the Monte Carlo mass distribution gives $M_{\gamma\pi}^{MC} = 80.6\ GeV$ with $\sigma = 6.2\ GeV$. The events from the data sample are therefore selected in the region $68\ GeV < M_{\gamma\pi} < 100\ GeV$ corresponding to the range between -2σ and 3σ.

For the 12 events which remain at this stage of the analysis the full tracking information from the central detectors is used. By requiring the presence of one and only one track and no preshower signal in a cone of 10° around the pion candidate cluster, no events remain in the data sample. The total efficiency, including geometrical acceptance, is evaluated to be $\varepsilon_{\gamma\pi}^{tot} = 0.072 \pm 0.004$, where the quoted error includes the statistical and systematic errors added in quadrature.

The upper limit on the amplitude ratio can be calculated as

$$R = \frac{\Gamma(W^{\pm} \rightarrow \pi^{\pm}\gamma)}{\Gamma(W^{\pm} \rightarrow e^{\pm}\nu)} = \frac{N_{\gamma\pi}^{prod}}{N_{e\nu}^{prod}} = \frac{N_{\gamma\pi}^{obs}/\varepsilon_{\gamma\pi}^{tot}}{N_{e\nu}^{prod}}$$

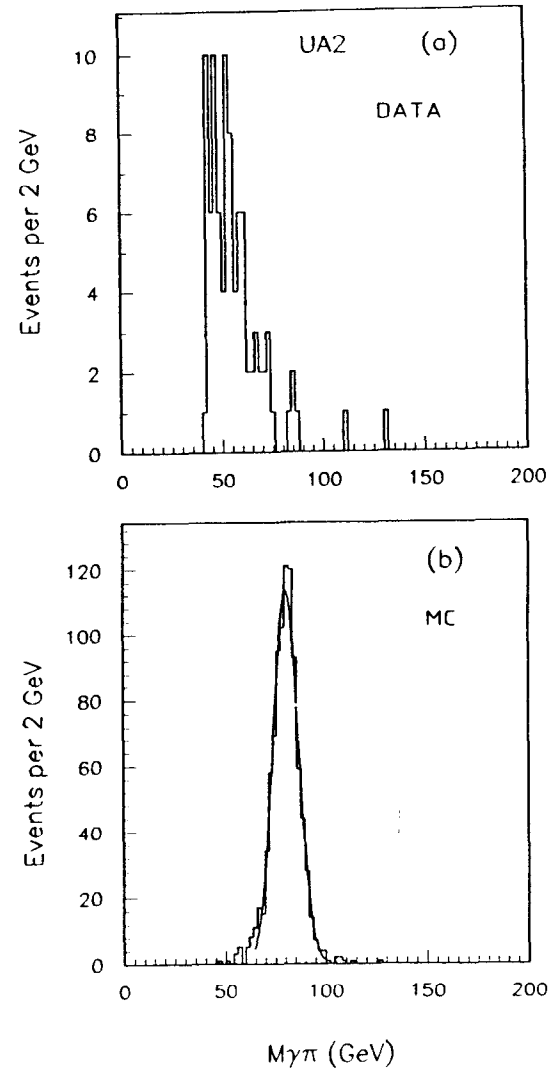

Figure 12: *Invariant mass of the $\gamma\pi$ system in the data (a) and Monte Carlo (b) samples after selections. The superimposed curve in (b) is the result of a Gaussian fit to the Monte Carlo mass distribution.*

where $N_{e\nu}^{prod} = 8539 \pm 444$ is given by the observed number of $W^{\pm} \to e^{\pm}\nu$ decays in UA2, corrected for the measured efficiency and acceptance [4]. The result is

$$R < 4.9 \cdot 10^{-3} \ (95\% \ CL) \ .$$

A limit on the branching ratio $Br(W^{\pm} \to \pi^{\pm}\gamma) = R \cdot Br(W^{\pm} \to e^{\pm}\nu)$ can be derived assuming the Standard Model value $Br(W^{\pm} \to e^{\pm}\nu) = 0.109$ as computed for $m_{top} > m_W - m_b$:

$$Br(W^{\pm} \to \pi^{\pm}\gamma) < 5.4 \cdot 10^{-4} \ (95\% \ CL) .$$

This result is similar to the limit obtained by LEP experiments [33] for the branching ratio of the decay $Z \to \pi^0\gamma$ which is also suppressed in the Standard Model.

5.2 Search for scalar leptoquarks

The symmetry between lepton and quark generations in the Standard Model naturally inspires the hypothesis of the existence of *leptoquarks (S)*, particles carrying both lepton and quark quantum numbers. In several models [34] leptoquarks can have masses m_S lower than 100 GeV and could be accessible at the CERN $\bar{p}p$ Collider. The leptoquark quantum numbers are model-dependent. The present search considers only scalar leptoquarks. It is assumed that each generation has its own leptoquark and that couplings occur only within a given generation [35].

In $\bar{p}p$ collisions, one expects single leptoquark as well as pair production. Single production is proportional to the model dependent quark–lepton–leptoquark ($q\ell S$) coupling, while in pair production only the contribution from the t-channel $q\bar{q}$ annihilation is affected by this dependence. Pair production is then expected to dominate [36] and, since the t-channel contribution is small and can be neglected, no assumption is needed about the $q\ell S$ coupling, nor the leptoquark charge.

The first family of leptoquarks is expected to manifest itself with decays containing a light quark and an electron (or positron) with a branching ratio b, or a light quark and a neutrino with a branching ratio $(1-b)$. The experimental signatures consist therefore in 2 charged leptons + 2 jets, 1 charged lepton + 2 jets + ν and 2 jets + $\nu\bar{\nu}$ where the neutrino(s) would give rise to missing transverse momentum ($\not{p}_T$) which can be experimentally measured.

• The two electron + jets channel

The search has been based on the data sample used to study $Z \to e^+e^-$ decays. Standard electron identification criteria have been applied to electromagnetic clusters in $|\eta| < 2$. After this selection 678 events were left. In order to suppress the background expected from Z + jets, Drell-Yan processes and misidentified electrons from QCD jet production, the two electrons were required to have $E_T >$ 18 GeV and $E_T > 9$ GeV respectively. In addition, at least two jets reconstructed within a cone radius of 0.7 in the $\eta - \phi$ space and with $E_T > 10$ GeV were required. After these criteria the data sample contained 9 events, all falling into an electron mass region between 80 and 100 GeV compatible with Z + 2 jet production. Thus by excluding this mass region from the search, no event was left in the data sample.

• The electron + jets + $\not{p}_T$ channel

Standard electon identification criteria have been applied to events having an electromagnetic cluster. Further selections were applied to the 4619 events left in order to reduce the background, which mainly arises from the associated production of W bosons and jets : $E_T > 15(20)$ GeV for the electron candidates in the 1988/89 (1990) data samples, $\not{p}_T > 20$ GeV, a tranverse mass $m_T > 25$ GeV of the electron–neutrino pair and at least two jets with $E_T > 20$ GeV in the pseudorapidity range $|\eta| < 2$ were required. After this selection 6 events were left in the data sample. They all had m_T in the range between 60 and 90 GeV, compatible with QCD calculations of W + 2-jet production. After the events with 60 $GeV < m_T <$ 90 GeV were rejected, no event was left in the data sample.

The expected detector response and the acceptance for leptoquark production were investigated with detailed Monte Carlo simulations as described in ref. [23]. For each channel the calculated acceptance was folded with the appropriate efficiencies. The combination of all the systematic uncertainties discussed in ref. [23] gives relative errors on the acceptance of 21.7% in the one–electron channel and of 20.3% in the two–electron channel. The estimated systematic uncertainties were added in quadrature, and the overall detection efficiency was reduced by the full error. The expected rates were then calculated using these "reduced" efficiency values.

No candidate events likely to have resulted from leptoquark pair production were observed in either of the two decay channels considered in this analysis. The maximum cross section σ^{MAX} compatible with this search allows the setting of a limit on the leptoquark mass, since

$$N_{CL} = \left[\varepsilon_{ee}\, b^2 + 2\,\varepsilon_{e\nu}\, b\,(1-b)\right] L\, \sigma^{MAX}$$

where N_{CL} is the number of events corresponding to the chosen confidence level, b is the branching ratio for the decay mode into an electron, ε_{ij} is the efficiency for the channel ij, (i and j stand for either e or ν), and L is the total integrated luminosity.

Figure 13 shows the lower limit on m_S at 95% CL as a function of b for the individual channels. The shaded area corresponds to the excluded region in the (b , m_S) plane. If one assumes a 50% branching ratio b, lower limits at 95% CL on the mass of first generation leptoquarks are determined to be 58 GeV from the electron–neutrino channel, 60 GeV from the electron–electron channel and 67 GeV from the two channels combined. A limit of 74 GeV is reached for $b = 100\%$.

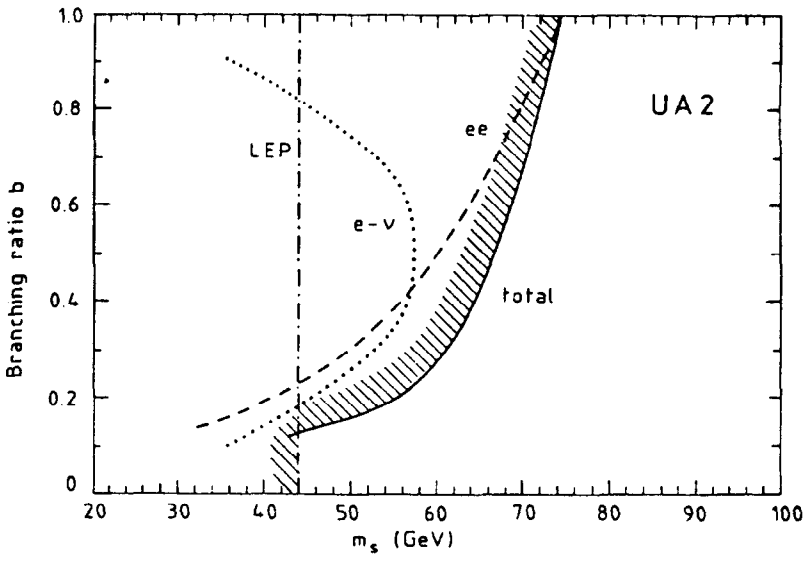

Figure 13: *Leptoquark mass limit at 95% CL as a function of the branching ratio b for the two-electron channel (ee), the electron-neutrino channel (eν) and for both channels combined. Also indicated is the limit obtained by the LEP experiments [36]. The shaded area represents the combined excluded mass region from UA2 and LEP experiments.*

5.3 Search for $H^{\pm}$ from top quark decay

Little experimental information exists on the nature of the Higgs sector of the Standard Model (SM). The simplest extensions beyond the minimal one-doublet version are models with two Higgs doublets [38], that require the existence of charged Higgs bosons ($H^{\pm}$). In such models the couplings of $H^{\pm}$ are fully specified by the parameters m_H and $tan\beta$ (where $tan\beta = v_2/v_1$ is the ratio of vacuum expectations for the two doublets). The existence of charged Higgs bosons can have important consequences for the discovery of the top quark since they would couple preferentially to heavy top. For $m_{top} > m_H$ the dominant decay modes of the H^+ would be $H^+ \to \tau\nu$ and $H^+ \to c\bar{s}$ with branching ratios depending on particle masses and $tan\beta$ values [24]. These final states were only recently searched for [39] and were not considered in the SM top searches at $\bar{p}p$ colliders [13, 40, 41]. It cannot be excluded therefore, that top could still be less massive than the W [38], with the lower bound on m_{top} given in section 3.4 from the measurements of Γ_W.

For $m_W > m_{top} + m_b$ and $m_{top} > m_H$ a search has been made for the decay

$$t \to H^+ b,\ H^+ \to \tau\nu,\ \tau \to hadrons\ +\ \bar{\nu} \qquad (1)$$

or its charge conjugate, with top produced via QCD processes or via $W \to t\bar{b}$. The analysis used the following method : first, the numbers of electrons and τ's in events with large missing transverse momentum $\not{p}_T$ are determined; the former is then used together with the assumption of $e - \tau$ universality to determine the number of τ's expected from IVB decays. This number is compared to the number of τ's observed in the data. An excess would indicate new physics whereas the absence of an excess makes it possible to exclude the $H^{\pm}$ for some values of the parameters of the model.

This analysis is based upon that used in the UA2 measurement of $e - \tau$ universality [42]. The data were obtained using a $\not{p}_T$ trigger in the 1988 and 1989 runs, while in the 1990 run a dedicated τ trigger was used [24] in order to reject di-jet events and the additional background to the τ signal from beam-gas interactions. The events were then selected by requiring $\not{p}_T > 20\ GeV$, $E_T^1 > 17\ GeV$, where E_T^1 is the transverse energy of the leading jet in the event, and no cluster with $E_T > 10\ GeV$ opposite to the leading one.

The τ candidates were selected on the basis of *hadronicity* (ξ) and *profile* (ρ) of the leading jet, where $\xi = E_{had}/E_{tot}$ is the ratio between the energy of the cluster contained in hadronic compartments (E_{had}) and the total cluster energy (E_{tot}), and ρ is the profile variable defined in section 5.1. Further requirements were applied to the leading cluster : cluster centroid in the fiducial region of the CC, $0.01 < \xi < 0.90$ and at least one track in a 10° cone about the cluster axis. A subdivision of the data into "$\tau + jets$" and "$\tau + 0\ jets$" subsamples then followed according to whether an additional cluster with $E_T > 10\ GeV$ did or did not appear in the event.

The selected samples contain the electrons from W decay, the τ's and a residual QCD jet background. To obtain estimates for the numbers of τ's one starts from the total number of events with a leading cluster at high profile, ($\rho > 0.75$), after rejecting events with an electromagnetic leading cluster. The numbers of events coming from beam-halo, jets and electrons are estimated and subtracted from the total. In each sample the number of electrons is estimated as in ref. [42], while the jet subtraction is performed by exploiting the differences in the profile distributions for jets and τ's as discussed in refs. [24, 42]. The final samples are then corrected for efficiencies and contributions from other sources of electrons and hadronic τ decays (e.g., $Z \to \tau^+\tau^-$).

The best estimate of the $e-\tau$ universality is obtained, as in ref. [42] using the "$\tau + 0$ *jets*" sample alone, with higher $\not{p}_T$ and E_T^1 thresholds (25 and 22 GeV, respectively) and a lower threshold of 2.5 GeV for the cluster opposite to the leading jet. The final result for the full sample is

$$\frac{g_\tau^W}{g_e^W} = 1.02 \pm 0.04(stat) \pm 0.04(syst).$$

When using the thresholds given above for the charged Higgs analysis, choosen for better acceptance, a slightly less precise result is obtained :

$$\frac{g_\tau^W}{g_e^W} = 0.99 \pm 0.06(stat) \pm 0.04(syst).$$

Using the number of observed electrons and the assumption that the ratio of couplings of the electron and τ to the W is strictly unity, estimates are obtained for the expected numbers of τ's from $W \to \tau\nu$ in the samples; the τ's coming from Z decay are taken into account as in [42]. These are then compared to the numbers of τ's observed in order to obtain the values for the τ excesses which are listed in Table 2.

Sample	τ's Expected	τ's Observed	Excess τ's
$\tau + 0$ *jet*	$760 \pm 31 \pm 25$	$754 \pm 68 \pm 54$	$-6 \pm 75 \pm 60$
$\tau + jets$	$68 \pm 8 \pm 3$	$73 \pm 24 \pm 5$	$+5 \pm 25 \pm 6$

Table 2: *Excess τ's in events with large $\not{p}_T$.*

To compare these numbers with what one would expect if the charged Higgs hypothesis were valid, the PYTHIA [31] event generator was used together with the UA2 detector simulation, to generate events with 16 different choices of m_H and m_{top}, in the range 44 $GeV < m_H <$ 66 GeV and 50 $GeV < m_{top} <$ 71.5 GeV. The number of τ's expected for each case was determined by applying the analysis cuts and normalizing to the production cross sections for top [40] and to the total integrated luminosity of 13 pb^{-1}. The systematic uncertainties in the numbers of τ's expected from W decay and of τ's observed are discussed in refs. [24, 42]. For τ's from $H^\pm$ the contributions from theoretical, Monte Carlo and experimental sources have been taken into account.

The observed excesses for the two samples are consistent with zero : it is now possible to ask whether this result is sufficient to exclude the existence of $H^\pm$ for some values of the parameters. For this purpose, levels of confidence for the exclusion of the process (1) for each of the 16 mass sets used in the Monte Carlo and for branching ratio (B) values of 0.5 and 1.0 (corresponding to $tan\beta$ values above roughly 1.0 and 2.0, respectively) were calculated. By interpolating the CL's for the 16 mass points, it is possible to define regions in the (m_H, m_{top}) plane which are exluded at 90 and 95 % CL. These are shown in Figure 14 (a) and (b) respectively. The regions excluded by UA1 [39] are also shown as are the model independent lower bounds for m_{top} from hadron collider measurements of Γ_W [4, 11, 12] and for m_H from LEP [43].

6 Conclusions

The UA2 detector has collected an integrated luminosity of 13.0 pb^{-1} between 1988 and 1990. The final W and Z samples gave an improved measurement of Standard Model parameters :

$$\Gamma_W = 2.10 \pm 0.16\ GeV$$

$$m_W = 80.35 \pm 0.33 \pm 0.17\ GeV$$

$$sin^2\theta_W = 0.2234 \pm 0.0064 \pm 0.0033.$$

Results on single photon inclusive cross section are well described by next-to-leading order QCD calculations. A search for $W^\pm \to \pi^\pm\gamma$ has led to the limit $Br(W^\pm \to \pi^\pm\gamma) < 5.4 \cdot 10^{-4}$ at 95% CL. A lower limit is determined for the mass of first generation scalar leptoquarks : $m_S > 67\ GeV$ at 95% CL. Finally, the decay $t \to H^+b$, $H^+ \to \tau\nu$, $\tau \to hadrons + \overline{\nu}$ and its charge conjugate, have been excluded in an extended region of the (m_H, m_{top}) plane for $B(H^\pm \to \tau\nu) = 0.5$ and 1.0.

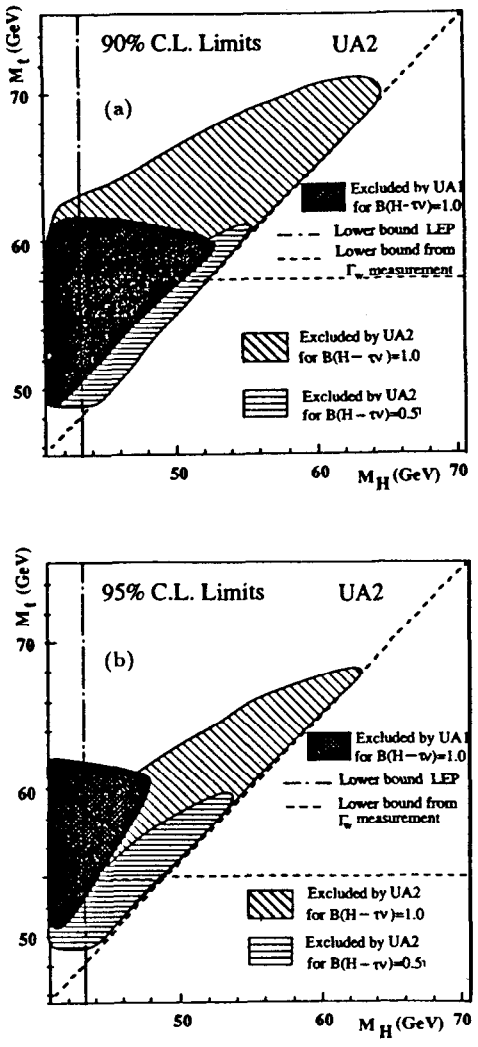

Figure 14: *Regions of the* $(m_H\ ,\ m_{top})$ *plane excluded at* 90% *CL (a) and* 95% *CL (b).*

References

[1] UA2 Collaboration, C.N. Booth, *Proc. 6th Topical Workshop on Proton-Antiproton Collider Physics* (Aachen, 1986), eds. K. Eggert et al.,(World Scientific, Singapore, 1987) p. 381.

[2] A. Beer et al., *Nucl. Instrum. Methods* **A224** (1984) 360.

[3] G. Blaylock et al., *Proc. Intern. Conf. on the Impact of Digital Microelectronics and Microprocessors on Particle Physics*, eds. M. Budinich et al., (World Scientific, Singapore, 1988) 247;
P. Baehler et al., ibid., 254.

[4] UA2 Collaboration, J. Alitti et al., CERN-PPE/91-162 (30 September 1991), submitted to *Physics Letters B.*

[5] R. Hamberg, W.L. Van Nerveen and T. Matsuura, *Nucl. Phys.* **B359** (1991) 343.

[6] UA2 Collaboration, J. Alitti et al., CERN-PPE/91-163 (30 September 1991), submitted to *Physics Letters B.*

[7] P.N. Harriman, A.D. Martin, R.G. Roberts and W.J. Stirling, *Phys. Rev.* **D42** (1990) 798 and *Phys. Lett.* **B243** (1990) 421.

[8] H. Plothow-Besch, *Parton Density Functions*, Proceedings of the 3rd Workshop on Detector and Event Simulation in High Energy Physics (Amsterdam, April 1991).

[9] CDF Collaboration, F. Abe et al., *Phys. Rev. Lett.* **65** (1990) 2243 and *Phys. Rev.* **D43** (1991) 2070.

[10] J. Carter, summary talk at *Lepton-Photon Symposium and Int. Europhysics Conference on High Energy Physics* (Geneva, July-August 1991).

[11] CDF Collaboration, F. Abe et al., *Phys. Rev. Lett.* **64** (1990) 152.

[12] UA1 Collaboration, C. Albajar et al., *Phys. Lett.* **B253** (1991) 503.

[13] K. Sliwa, in *High Energy Hadron Interactions*, proceedings of the XXVth Rencontres de Moriond, Les Arcs, France, edited by J. Tran Thanh Van (Editions Frontieres, Gif-sur-Yvette, 1990).

[14] A. Sirlin, *Phys. Rev.* **D22** (1980) 971.

[15] G.L. Fogli, D. Haidt, *Z. Phys.* **C40** (1988) 379.

[16] UA2 Collaboration, J. Alitti et al., *Phys. Lett.* **B263** (1991) 544.

[17] P. Aurenche et al., *Phys. Lett.* **B140** (1984) 87;
P. Aurenche et al., *Nucl. Phys.* **B297** (1988) 661.

[18] R. Ford and W. Nelson, SLAC-210 (1978).

[19] UA2 Collaboration, M. Banner et al., *Z. Phys.* **C27** (1985) 329.

[20] D.W. Duke and J.F. Owens, *Phys. Rev.* **D30** (1984) 49;
E. Eichten et al., *Rev. Mod. Phys.* **56** (1984) 579 and erratum *Rev. Mod. Phys.* **58** (1986) 1065;
P. Aurenche et al., *Phys. Rev.* **D39** (1989) 3275.

[21] UA2 Collaboration, J. Alitti et al., *Phys. Lett.* **257B** (1991) 232.

[22] UA2 Collaboration, J. Alitti et al., CERN-PPE/91-208 (18 November 1991), submitted to *Physics Letters B.*

[23] UA2 Collaboration, J. Alitti et al., CERN-PPE/91-158 (25 September 1991), submitted to *Physics Letters B.*

[24] UA2 Collaboration, J. Alitti et al., *A search for charged Higgs from Top quark decay at the CERN $\bar{p}p$ Collider*, in preparation for *Physics Letters B.*

[25] UA2 Collaboration, J. Alitti et al., *Z. Phys.* **C49** (1991) 17.

[26] L. Arnellos, W.J. Marciano and Z. Parsa, *Nucl. Phys.* **B196** (1982) 378.

[27] M. Jacob and T.T. Wu, *Phys. Lett.* **B232** (1989) 529.

[28] S. Gosh and D. Chatterjee, *Mod. Phys. Lett.* **A5** (1990) 1493.

[29] A.V. Manohar, *Phys. Lett.* **B244** (1990) 101;
T. Schröder, *Europhys. Lett.* **12** (1990) 497;
N.G. Deshpande, et al., *Phys. Lett.* **B241** (1990) 119;
K. Hikasa, *Mod. Phys. Lett.* **A5** (1990) 1801;
T.N. Pham, *Phys. Lett.* **B247** (1990) 438.

[30] UA1 Collaboration, C. Albajar et al., *Phys. Lett.* **B241** (1990) 283.

[31] H.U. Bengtsson and T. Sjöstrand, PYTHIA, *Comput. Phys. Commun.* **46** (1987) 43.

[32] T. Sjöstrand, private communication.

[33] ALEPH Collaboration, D. Decamp et al., *Phys. Lett.* **B241** (1990) 635;
ALEPH Collaboration, D. Decamp et al., CERN-PPE/91-149 (20 September 1991), submitted to *Physics Reports*;
DELPHI Collaboration, P.Abreu et al., CERN-PPE/91-109 (5 July 1991), submitted to *Physics Letters B*;
L3 Collaboration, B. Adeva et al., *Phys. Lett.* **B250** (1990) 199;
OPAL Collaboration, M.Z. Akrawy et al., *Phys. Lett.* **B241** (1990) 133;
OPAL Collaboration, M.Z. Akrawy et al., *Phys. Lett.* **B257** (1990) 531.

[34] W. Buchmüller and D. Wyler, *Phys. Lett.* **B177** (1986) 377;
V. D. Angelopulos et al., *Nucl. Phys.* **B292** (1987) 59.

[35] J. L. Hewett and S. Pakvasa, *Phys. Rev.* **D37** (1988) 3165 and Refs. therein.

[36] J. L. Hewett and T. G. Rizzo, *Phys. Rev.* **D36** (1987) 3367.

[37] ALEPH Collaboration, D. Decamp et al., CERN-PPE/91-149 (1991);
DELPHI Collaboration, P. Abreu et al., CERN-PPE/91-137 (1991);
L3 Collaboration, B. Adeva et al., L3 preprint 26 (1991);
OPAL Collaboration, G. Alexander et al., *Phys. Lett.* **B263** (1991) 123.

[38] S.L. Glashow and E. Jenkins, *Phys. Lett.* **B196** (1987) 233.

[39] UA1 Collaboration, C. Albajar et al., *Phys. Lett.* **B257** (1991) 459.

[40] UA2 Collaboration, J. Alitti et al., *Z. Phys.* **C46** (1990) 1.

[41] UA1 Collaboration, C.Albajar et al., *Z. Phys.* **C48** (1990) 1.

[42] UA2 Collaboration, J. Alitti et al., CERN-PPE/91-69 (15 April 1991), submitted to *Z. Phys.* **C**.

[43] ALEPH Collaboration, D. Decamp et al., *Phys. Lett.* **B 241** (1990) 623;
ALEPH Collaboration, D. Decamp et al., *Phys. Lett.* **B 236** (1990) 511;
DELPHI Collaboration, P. Abreu et al., *Phys. Lett.* **B 242** (1990) 542;
L3 Collaboration, B. Adeva et al., *Phys. Lett.* **B 252** (1990) 511;
OPAL Collaboration, M.Z. Akrawy et al., *Phys. Lett.* **B 242** (1990) 299;
OPAL Collaboration, M.Z. Akrawy et al., *Phys. Lett.* **B 236** (1990) 364.